A multi-disciplinary investigation of the AFEN Slide: the relationship between contourites and submarine landslides

Ricarda Gatter[1]*, Michael A. Clare[2], James E. Hunt[2], Millie Watts[2], B. N. Madhusudhan[3], Peter J. Talling[4] and Katrin Huhn[1]

[1]MARUM – Center for Marine Environmental Sciences, University of Bremen, Leobener Str. 8, 28359, Germany

[2]University of Southampton, Engineering, Southampton Boldrewood Innovation Campus, Burgess Road, Southampton SO16 7QF, UK

[3]National Oceanography Centre, University of Southampton Waterfront Campus, Southampton European Way, Southampton, SO14 3ZH, UK

[4]University of Durham, Departments of Earth Sciences and Geography, Durham, DH1 3LE, UK

RG, 0000-0001-6548-4534; BNM, 0000-0002-2570-5934
*Correspondence: rgatter@marum.de

Abstract: Contourite drifts are sediment deposits formed by ocean bottom currents on continental slopes worldwide. Although it has become increasingly apparent that contourites are often prone to slope failure, the physical controls on slope instability remain unclear. This study presents high-resolution sedimentological, geochemical and geotechnical analyses of sediments to better understand the physical controls on slope failure that occurred within a sheeted contourite drift within the Faroe–Shetland Channel. We aim to identify and characterize the failure plane of the late Quaternary landslide (the AFEN Slide), and explain its location within the sheeted drift stratigraphy. The analyses reveal abrupt lithological contrasts characterized by distinct changes in physical, geochemical and geotechnical properties. Our findings indicate that the AFEN Slide likely initiated along a distinct lithological interface, between overlying sandy contouritic sediments and softer underlying mud-rich sediments. These lithological contrasts are interpreted to relate to climatically controlled variations in sediment input and bottom current intensity. Similar lithological contrasts are likely to be common within contourite drifts at many other oceanic gateways worldwide; hence our findings are likely to apply more widely. As we demonstrate here, recognition of such contrasts requires multi-disciplinary data over the depth range of stratigraphy that is potentially prone to slope failure.

Thermohaline-driven ocean bottom currents create sedimentary accumulations called contourites that are found along the world's continental margins (e.g. McCave and Tucholke 1986; Rebesco and Stow 2001; Stow *et al.* 2002). Contourites can cover extremely large areas (from <100 km² to >100 000 km²), forming a variety of depositional geometries that include elongated, mounded, sheeted, channelized and mixed drift systems (Faugères *et al.* 1999; Rebesco and Stow 2001; Stow *et al.* 2002; Faugères and Stow 2008). It has become increasingly apparent that contourite drifts are prone to slope instability (Laberg and Camerlenghi 2008), with submarine landslides recognized in a wide range of locations affected by bottom currents (Table 1).

The affinity of contourite drifts for slope failure can be linked in part to deposit morphology (Fig. 1, Table 1). In some locations, contour-parallel currents modify the continental slope profile, creating mounded accumulations of sediment that are

thicker and steeper than those on slopes unaffected by bottom currents (Laberg and Camerlenghi 2008; Rebesco *et al.* 2014). Factors such as sediment supply, intensity and location of currents, and sea-level and climatic changes control the presence or absence, location, growth and morphology of contourites (Faugères and Stow 2008; Rebesco *et al.* 2014). A number of compound morphological effects have been implicated as preconditioning and/or triggering mechanisms for slope instability. These include (1) slope over-steepening due to rapid sediment accumulation (A, Fig. 1) or due to erosion by vigorous along-slope currents (B, Fig. 1) and (2) loading resulting from differential sediment accumulation (C, Fig. 1). These effects occur particularly where contourites form as mounded accumulations (Laberg and Camerlenghi 2008; Prieto *et al.* 2016; Miramontes *et al.* 2018). However, submarine landslides, some of which include the largest on our planet (e.g. Storegga; Bryn *et al.* 2005*a*), often occur

Table 1. *Examples of submarine landslides in contourites*

Slide name	Location	Setting	Slide volume (km³)	Seabed gradient (°)	Sediment accumulation rate	Drift type	Main control	References
Hinlopen-Yermak Slide	Northern Svalbard margin, Arctic Ocean	Northern high-latitudes	1200–1350	<0.5		?	Lithological and geotechncial contrasts	Vanneste *et al.* (2006), Winkelmann *et al.* (2008)
Fram Slide Complex	Offshore northwest Svalbard, Arctic Ocean	Northern high-latitudes	*c.* 1470 (17 failures)	*c.* 1.5–4.5	3–19 cm ka⁻¹	Plastered drift	Toe erosion, morphology	Mattingsdal *et al.* (2014), Elger *et al.* (2017)
–	Lofoten Islands, offshore Norway, Norwegian Sea	Northern high-latitudes	<1–8.7 (individual landslides)	4–1	Up to 4 m ka⁻¹	Mounded, elongated drift (Lofoten drift)	Under-cutting	Laberg *et al.* (2001), Baeten *et al.* (2013, 2014)
Trænadjupet Slide	Offshore Norway, Norwegian Sea	Northern high-latitudes	*c.* 900	2.3–0.6	Up to 65 m ka⁻¹	Mounded, elongated drift (Nyk drift)	Weak layer	Laberg and Vorren (2000), Laberg *et al.* (2001, 2002, 2003)
Nyk Slide	Offshore Norway, Norwegian Sea	Northern high-latitudes			Up to 1.2 m ka⁻¹	Mounded, elongated drift (Nyk drift)	Weak layer	Laberg *et al.* (2001, 2002), Lindberg *et al.* (2004)
Sklinnadjuped Slide	Offshore Norway, Norwegian Sea	Northern high-latitudes			Up to 0.5 m ka⁻¹	Infilling drift (Sklinnadjuped drift)	Weak layer (?)	Laberg *et al.* (2001), Dahlgren *et al.* (2002)
Storegga Slide	Offshore Norway, Norwegian Sea	Northern high-latitudes	2400–3200	0.5–1.0		Mounded, elongated drift	Sensitive clay layer	Bryn *et al.* (2005a, b), Haflidason *et al.* (2005), Kvalstad *et al.* (2005)
Tampen Slide	Offshore Norway, Norwegian Sea	Northern high-latitudes				Mounded elongated drift (?)		Evans *et al.* (2005), Solheim *et al.* (2005)
Northern Faroe Slide Complex	Faroe Islands, offshore UK, Norwegian Sea	Northern high-latitudes			14–30 cm ka⁻¹	Mounded, elongated drift (Faroe drift)		Rasmussen *et al.* (1996, 1998), Van Weering *et al.* (1998), Kuijpers *et al.* (2001), Long *et al.* (2004)
AFEN Slide	Offshore UK, Faroe–Shetland Channel	Northern high-latitudes	*c.* 0.153 (all phases)	1–3	Up to 10 cm ka⁻¹	Sheeted to mounded drift (West Shetland drift)	Sandy layer (?)	Knutz and Cartwright (2004), Wilson *et al.* (2004)
Rockall Bank Slide Complex	Offshore Ireland, Rockall Trough	Northern high-latitudes	265–765	5–10	5–17.1 cm ka⁻¹	Elongated, mounded drift (Feni drift)	Weak layers	Van Weering and de Rijk (1991), Faugères *et al.* (1999), Georgiopoulou *et al.* (2013, 2019)
–	Offshore eastern Canada, North Atlantic	Northern mid-latitudes				Plastered drift (?)		Piper (2005)
–	Grand Banks, offshore eastern Canada, North Atlantic	Northern mid-latitudes		2	Up to 50 cm ka⁻¹	Plastered drift	Lithological and geotechnical contrasts	Rashid *et al.* (2017)

	Location	Latitude	Slide volume	Seabed gradient	Sediment accumulation rate	Drift type	Main controls	References
–	Pianosa Ridge, Mediterranean Sea	Northern mid-latitudes		3–10 (locally 20)	13 cm ka^{-1}	Plastered drift	Over-steepening	Miramontes *et al.* (2016, 2018)
–	Gela and south Adriatic Basin, Mediterranean Sea	Northern mid-latitudes	0.1–0.2 (individual mass transport deposits)	*c.* 3	22.5 cm ka^{-1}	Elongated and separated drifts	Mechanical boundary, clay layer	Minisini *et al.* (2007), Verdicchio and Trincardi (2008)
–	SW Mallorca Island, Mediterranean Sea	Northern mid-latitudes		1.3–2.9	5.8 cm ka^{-1} (?)	Mounded, elongated drifts		Lüdmann *et al.* (2012)
–	Alboran Sea, Mediterranean Sea	Northern mid-latitudes				Contourite despositional system		Ercilla *et al.* (2016)
–	Levant Basin, Mediterranean Sea	Northern mid-latitudes	Generally, <1 (individual landslides)	>4	25–130 cm ka^{-1}	Plastered drift	Over-steepening	Katz *et al.* (2015), Hübscher *et al.* (2016)
–	Bahamas Bank	Norther low-latitudes	2–20 (individual landslides)	*c.* 3		Plastered drift	Stratigraphic control (?)	Mulder *et al.* (2012); Principaud *et al.* (2015), Tournadour *et al.* (2015)
–	Offshore Uruguay	Southern mid-latitudes	<2 (individual landslides)	1–3	8–18 cm ka^{-1}	Contourite depositional system	Lithological control	Henkel *et al.* (2011), Krastel *et al.* (2011), Ai *et al.* (2014), Hernández-Molina *et al.* (2016)
–	Offshore Argentina	Southern mid-latitudes		3–7	Up to 1.6 m ka^{-1}	Contourite depositional system	Lithological control; over-steepening	Hernández-Molina *et al.* (2009), Ai *et al.* (2014), Krastel *et al.* (2011), Preu *et al.* (2013)
–	Offshore Antarctic Peninsula, Pacific Ocean	Southern low-latitudes		2–3	Decrease from 18 to *c.* 8 cm ka^{-1}	Mounded drifts	Under-cutting; weak layer	Iwai *et al.* (2002), Volpi *et al.* (2003, 2011)

Slide volume, seabed gradient and sediment accumulation rate are given where available. Main controls of slope failure are listed where they are known or discussed in the literature.

R. Gatter *et al.*
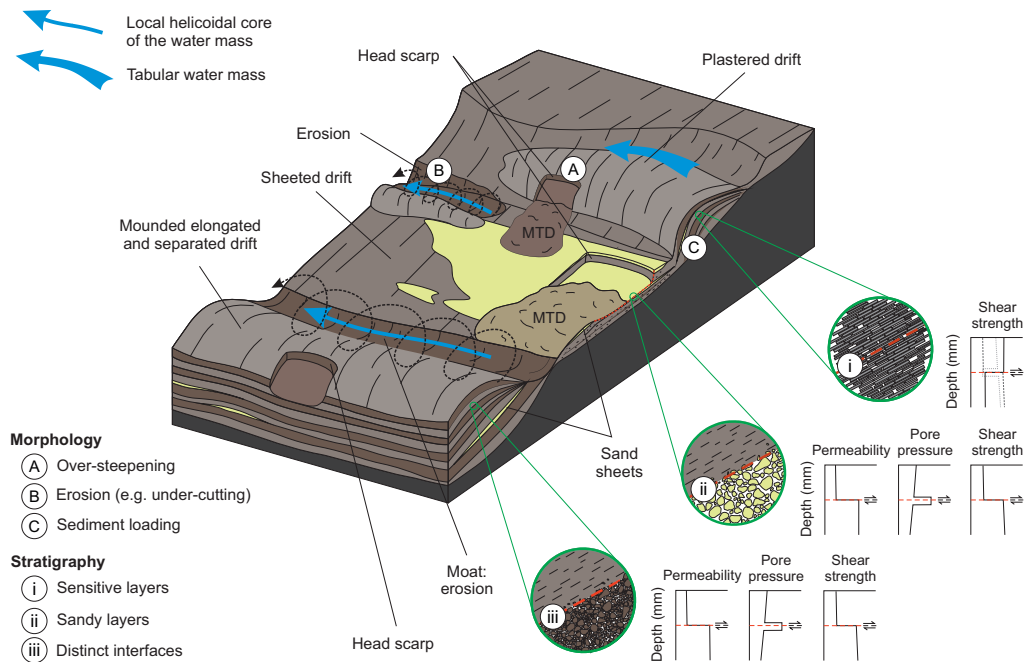
Fig. 1. Key characteristics of contourites that favour the formation of submarine landslides. Morphological controls: (A) over-steepening, (B) erosion, (C) sediment loading; stratigraphic controls: (i) laterally extensive sensitive clay layers that are prone to sudden strength loss, possible shear strength depth profiles are shown as black; dark grey, dashed and light grey, dotted lines; (ii) thick accumulation of sandy layers that can accommodate excess pore pressure due to high sedimentation rates; (iii) distinct lithological and/or geotechnical interfaces. Contourite depositional system adopted from Hernández-Molina *et al.* (2008).

within contourite drifts on very low angle (<2°) slopes (e.g. Hühnerbach *et al.* 2004). Another explanation for slope instability in contourite drifts, therefore, relates to specific compositional and geotechnical properties of contourites (Fig. 1, Table 1; Lindberg *et al.* 2004; Kvalstad *et al.* 2005). Plausible controls include prominent layers within the slope stratigraphy (Fig. 1) that may feature a lower peak or post-peak shear strength than over- and underlying strata, such as (i) laterally extensive (sometimes cm-thin) homogeneous layers of weaker, sensitive material that is prone to sudden strength loss (e.g. sensitive clay in the Storegga Slide, Norway – Kvalstad *et al.* 2005; sensitive zeolite layer in the N Tyrrhenian Sea – Miramontes *et al.* 2018), or (ii) thick accumulations of sandy material that is characterized by high sedimentation rates, promoting excess pore pressure (Laberg and Camerlenghi 2008; Ai *et al.* 2014). Another plausible control relates to lithological and/or geotechnical contrasts within a depositional sequence that may result from rapid changes in current regime, sediment input or type (e.g. Rashid *et al.* 2017; see (iii) on Fig. 1).

Detailed sedimentological and geotechnical studies of landslides within contourites are scarce (Baeten *et al.* 2013; Miramontes *et al.* 2018), and

there is still much uncertainty as to which specific aspects act as the dominant control on slope instability. Many studies rely solely upon remote geophysical data for landslide characterization and, if sediment cores are acquired, they typically do not penetrate to the failure plane (which may be tens to hundreds of metres below the seafloor; Talling *et al.* 2014). Such cores also tend to focus on characterization of the failed landslide mass, rather than targeting sediments from adjacent undisturbed slopes. Targeting the undisturbed sediments of the adjacent slopes, including those stratigraphically equivalent to the failure plane of the landslide, however, is necessary in order to identify and characterize the material along which the landslide initiated, as these are usually removed or remoulded during failure. It is of critical importance to be able to identify sediments that are prone to failure in order to perform reliable slope stability assessments (L'Heureux *et al.* 2012; Vardy *et al.* 2012).

Aims

Here, we present a detailed characterization of a bedding-parallel, cohesive submarine landslide

(called the AFEN Slide), which occurred within a low angle (<2.5°) laterally extensive sheeted contourite drift, based on physical, geochemical, sedimentological and geotechnical analyses. We focus on a sediment core targeted to sample the pre-landslide sedimentary sequence, including sediments that correlate stratigraphically with the failure plane located further upslope. Based on centimetre-resolution characterization of these deposits we address the following questions: first, what is the nature of the undisturbed sediment and do material heterogeneities explain the location of the failure plane? As many aspects of cohesive landslides appear to be scale invariant, this study of a relatively small landslide may provide key insights into our understanding of much larger ones (Micallef *et al.* 2008; Chaytor *et al.* 2009; Baeten *et al.* 2013; Casas *et al.* 2016; Kuhlmann *et al.* 2017; Clare *et al.* 2018). Second, what causes the observed heterogeneities within the stratigraphy? We explore how climatic changes and ocean circulation may play a key role in governing not just the failure plane depth, but also influence the timing of slope failure. Finally, we discuss the implications of climatically controlled sediment supply and deep ocean circulation for pre-conditioning slope instability in contourite depositional systems in oceanic gateways, which are narrow, deep passages connecting adjacent basins, elsewhere in the world.

Background

Regional setting

Geological and morphological setting. The study area lies on the eastern margin of the Faroe–Shetland Channel, which is located north of Scotland, extending over 400 km between the Wyville–Thomson Ridge and the Norwegian Basin (Fig. 2). The Faroe–Shetland Channel is a narrow basin, measuring 250 km at its widest in the NE and less than 130 km in the SW. The channel closely follows the trend of the regional NE–SW structural lineaments, and one of the NW–SE transfer zones (Victory Transfer Zone) passes close to the study area (Rumph *et al.* 1993; Wilson *et al.* 2004). The Faroe–Shetland Channel is the present-day expression of the Faroe–Shetland Basin that can be dated back to the Late Paleozoic (e.g. Rumph *et al.* 1993). Basin formation was probably initiated during the Devonian, while the main rift phase occurred during Cretaceous times (Dean *et al.* 1999; Roberts *et al.* 1999). Although localized extension continued until the early to mid-Paleocene (Smallwood and Gill 2002), more or less continuous post-rift subsidence predominated throughout the Cenozoic (Turner and Scrutton 1993). This subsidence was interrupted at various stages by

contractional deformation (Ritchie *et al.* 2003, 2008; Johnson *et al.* 2005; Stoker *et al.* 2005) and regional uplift and tilting (Andersen *et al.* 2000; Smallwood and Gill 2002; Stoker *et al.* 2002, 2005). Following Late Paleocene uplift, the Faroe–Shetland Channel subsided about 2000 m, with present-day water depths of 1700 m in the NE and 1000 m in the SW, and slope angles between 1° and 3° flanking the eastern channel margin (Stoker *et al.* 1998; Andersen *et al.* 2000; Smallwood and Gill 2002). The channel forms an important oceanic gateway, exchanging water masses between the North Atlantic and the Norwegian Sea (Broecker and Denton 1990; Rahmstorf 2002) since at least the Early Oligocene (Davies *et al.* 2001).

Oceanography and palaeoceanography. In general, the present-day oceanography in the Faroe–Shetland Channel consists of warm surface water moving towards the NE, and cold bottom water, generating relatively strong, erosive bottom currents (with velocities in the range between <0.3 and >1.0 m s^{-1}; Masson *et al.* 2004), moving towards the SW (Fig. 2a; Saunders 1990; Turrell *et al.* 1999; Rasmussen *et al.* 2002). Five distinct water masses can be recognized based on their salinity and temperature characteristics (Turrell *et al.* 1999). Two distinct surface water masses transport warm water from the North Atlantic into the channel. North Atlantic Water (NAW) flows northward from the Rockall Trough (Turrell *et al.* 1999), while Modified North Atlantic Water (MNAW) flows clockwise around the Faroe Islands before turning northward in the Faroe–Shetland Channel (Saunders 1990). These surface waters typically occupy the upper 200–400 m of the water column (Turrell *et al.* 1999). Arctic Intermediate Water (AIM) flows anticlockwise along the southern edge of the Norwegian Basin and around the Faroe–Shetland Channel, typically between 400 and 600 m water depth (Blindheim 1990). At the base of the channel (usually below 600 m water depth), the Norwegian Sea Arctic Intermediate Water (NSAIW) and the Faroe–Shetland Channel Bottom Water (FSCBW) are funnelled along the Faroe–Shetland Channel towards the south (Turrell *et al.* 1999) and flow along the Faroe Bank Channel into the Atlantic (Saunders 1990). A small portion of the cold bottom water flows across the western end of the Wyville–Thomson Ridge south into the Rockall Trough (Stow and Holbrook 1984). The velocity of these water masses is variable, both across the channel and over time. The average along-slope velocities, mainly directed NE, of around 0.2–0.25 m s^{-1} were measured at around 500–700 m water depth (Van Raaphorst *et al.* 2001; Bonnin *et al.* 2002) and velocities over >1.0 m s^{-1} associated with SW-directed bottom currents were inferred from observed bedforms (Masson *et al.* 2004). Periodic
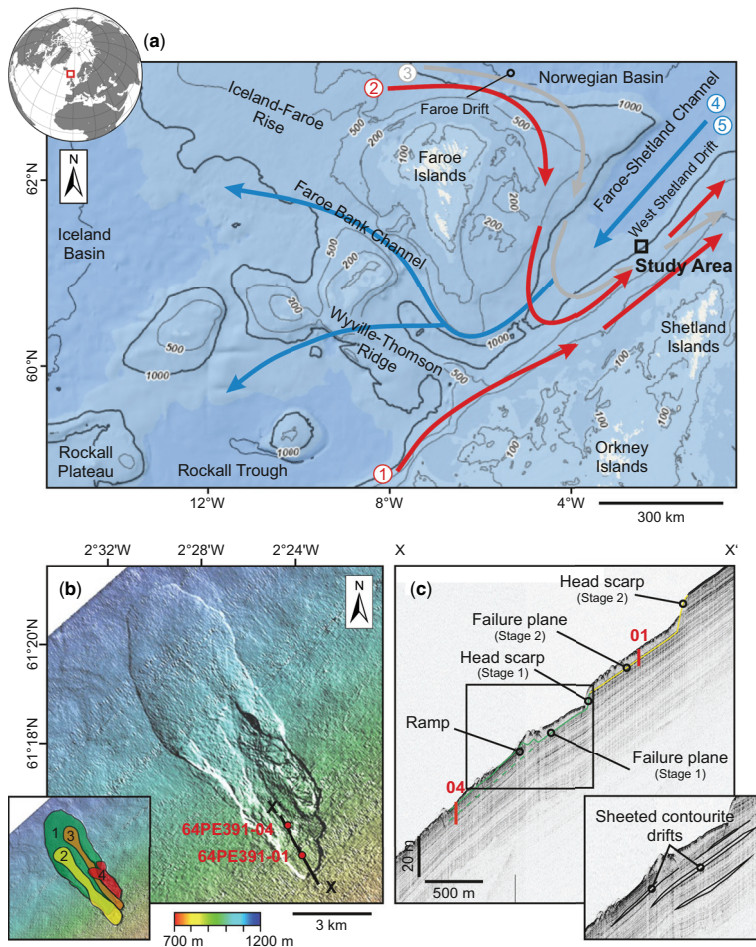
Fig. 2. (**a**) Schematic diagram of current regime in and around the Faroe–Shetland Channel. Arrows indicate the five main water masses: red 1, North Atlantic Water; red 2, Modified North Atlantic Water; grey 3, Arctic Intermediate Water; blue 4, Norwegian Sea Arctic Intermediate Water; blue 5, Faroe–Shetland Channel Bottom Water (after Turrell *et al.* 1999). The study area is outlined with a black square. (**b**) Outline of the AFEN Slide, showing piston core 64PE391-01 (61° 15′ 40.679″ N, 02° 23′ 42.899″ W; Madhusudhan *et al.* 2017) and Core 64PE391-04 (61° 16′ 17.651″ N, 02° 24′ 21.959″ W) as red circles. A black line illustrates the seismic line shown in (c). Inset image shows the four stages of the failure as interpreted by Wilson *et al.* (2004). Modified from Madhusudhan *et al.* (2017). (**c**) Seismic line across the AFEN Slide showing piston core 01 and 04. Inset image illustrates the distribution of sheeted contourite drifts in the area (after Wilson *et al.* 2004).

changes in salinity and temperature cause shifts of the boundaries between water masses on timescales from decades to hours (Turrell *et al.* 1999). Since the Last Glacial Maximum (LGM), when bottom and surface currents were weak, eight distinct changes in the surface and bottom current regime were identified, which are related to the changes in climatic conditions (Rasmussen *et al.* 2002). Climatic and palaeoceanographic changes also reportedly caused strong cyclical variation in sediment accumulation (with up to 30 cm ka^{-1} along the

Faroe Drift and up to 10 cm ka^{-1} along the West Shetland Drift; Rasmussen *et al.* 1996, 1998; Knutz and Cartwright 2004; Nielsen *et al.* 2007).

Contourite deposits in the Faroe–Shetland Channel

The regional oceanography has controlled the depositional architecture of the slope sediments, creating elongated mounded contourite drifts at the base of

the slope (to the NE of the AFEN Slide) and sheeted contourite drifts in the slide area (Long *et al.* 2004; Hohbein and Cartwright 2006). These sheeted drifts are characterized by parallel, laterally continuous reflectors on seismic profiles (Masson 2001). These reflectors can be traced over more than 50 km below the seafloor of the Faroe–Shetland Channel, which emphasizes the regional scale of bottom current activity and sheeted contourite drift accumulation (Stoker *et al.* 1998).

The AFEN Slide

The AFEN Slide was first identified in 1996, during an environmental survey for the Atlantic Frontiers Environmental Network in the region (Wilson *et al.* 2004). The slide is interpreted as a four-stage retrogressive landslide that occurred NW of the Shetland Islands (UK) at water depths of 830–1120 m on a slope varying from approximately 0.7° to about 2.5° (Wilson *et al.* 2003, 2004; Fig. 2b). The total length from the head scarp to the toe of the lobe is over 12 km, and the maximum width is around 4.5 km. The slide involved *c.* 200×10^6 m^3 of sediment and the slide debris has a maximum thickness of 20 m, averaging between 5 and 10 m (Wilson *et al.* 2004). Radiocarbon dating and biostratigraphy from the slide suggest that the first stage took place around 16–13 ka BP and the later retrogressive phases after 5.8 ka BP and prior to 2.8 ka BP (Wilson *et al.* 2004). Initial studies, based on high-resolution seismic data and sediment cores that did not penetrate the base of the slide, inferred that the failure plane comprised well-sorted contourite sands, which may liquefy during an earthquake (e.g. 10 000-year return period earthquake; Jackson *et al.* 2004). This hypothesis was supported by the presence of a buried slide, which appears to have occurred under similar physiographic conditions (Masson 2001; Wilson *et al.* 2003, 2004). Such well-sorted contourite sands were not found by Madhusudhan *et al.* (2017), who analysed a new sediment core (64PE391-01) that penetrated through the full extent of the deposits from the second stage of the landslide (Fig. 2c). Instead, they proposed progressive failure of geotechnically sensitive clays or liquefaction of silt layers. None of these previous cores sampled undisturbed material that corresponds stratigraphically with the failure plane.

Data and methods

Core 64PE391-04, which is the focus of this present study, was obtained during the RV *Pelagia* cruise 64PE391 in 2014 using a piston corer. The core was sampled within the AFEN Slide area, at a water depth of 945 m. It was targeted to sample undisturbed sediments, i.e. those characterized on seismic data by continuous reflectors and avoiding acoustically transparent, chaotic or disrupted seismic units and areas of hummocky seafloor texture likely indicative of slope failure (Shipp *et al.* 2011; Fig. 2). Figure 2 shows the location of core 64PE391-04 on the deep tow boomer seismic profile, which has a maximum theoretical vertical resolution of 0.5 m, with a penetration of 100 ms, and was obtained from the BGS 00/02 survey (Wilson *et al.* 2005). The core recovered 11.49 m of sediment in a 15 m core barrel and was kept in refrigerated storage at the British Ocean Sediment Core Facility (BOSCORF), UK, prior to study.

Physical properties analysis

A Geotek MSCL-S (Standard) multi-sensor core logger, based at BOSCORF, was used to measure P-wave velocity, gamma-ray bulk density, electrical resistivity, magnetic susceptibility and fractional porosity, which is derived from the measured sediment density at 1 cm intervals on split cores (Fig. 3). MSCL is a commonly used, non-destructive tool that allows the recognition of subtle changes in sediment physical properties. The data are commonly used for correlation between cores, and calibration of seismic data using P-wave velocity. Density serves as an effective proxy for changes in sediment lithology and is used for the calculation of fractional porosity (Gunn and Best 1998). Core images were obtained using the BOSCORF Geotek MSCL-CIS (Core Imaging System), which enables the acquisition of precise depth-registered images that can be correlated with the other datasets.

Geochemical analysis

Micro-XRF (X-ray fluorescence) core scanning was used to determine the geochemical composition of the sediment (ITRAX™ COX Ltd at BOSCORF; Croudace *et al.* 2006) at a spatial resolution of 1 cm. ITRAX scanning is a useful, rapid, non-destructive, high-resolution scanning technique that is widely used in earth and environmental sciences (Croudace and Rothwell 2015). This method enables the measurement of element intensities, such as Ca and Sr, which correlate well with the carbonate content, or Fe, Ti and K, which are related to the siliciclastic components, and vary directly with the terrigenous sediment input (e.g. Röhl and Abrams 2000; Hepp *et al.* 2006). ITRAX data represent a semi-quantitative analysis of the relative element abundances down-core. Data are expressed as counts per second (cps) and are presented as log ratios, which are accepted as a more accurate estimation of element concentrations. In addition, all XRF data are shown as log ratios of two elements, in order to show element concentrations more accurately
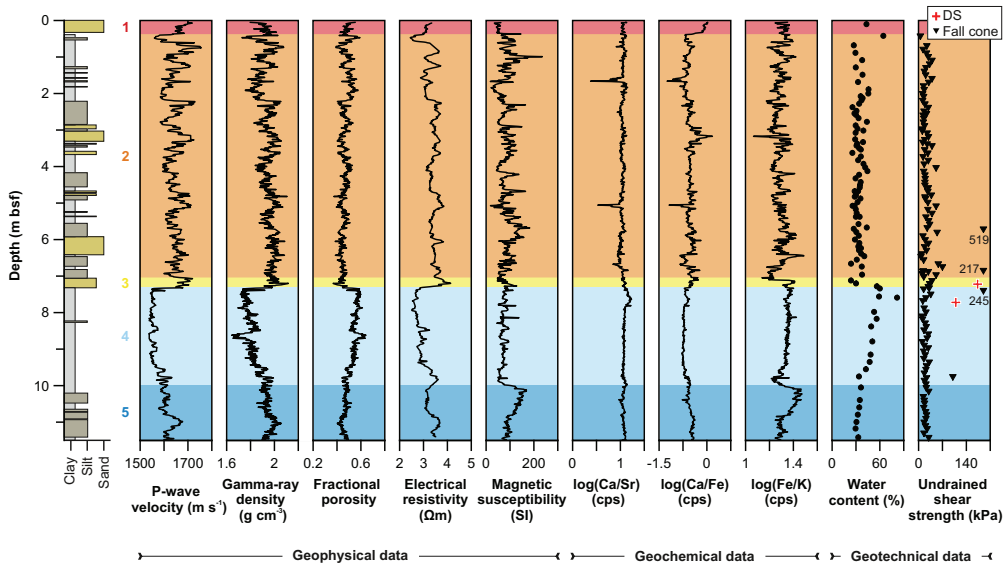
Fig. 3. Summary of sediment core analyses (64PE391-04), including visual sedimentary, physical properties (multi-sensor core logging) and geochemical (ITRAX X-ray fluorescence) core-log data, and geotechnical data (water content, drained and undrained shear strength). Units 1–5 are outlined.

and minimize matrix effects inherent to XRF (Weltje and Tjallingii 2008). Ca/Sr, Ca/Fe and Fe/K have been selected, as these element ratios have been shown to reflect changes in sea-level and temperature, sediment supply, and have been applied in climate studies (see Croudace and Rothwell 2015). In addition to geochemical composition, the ITRAX instrument provided X-radiographs. X-radiographs are digital images of the internal structure and physical property changes within a split core section that are obtained using optical and radiographic line cameras.

Grain-size distribution

Grain-size analysis was carried out at 10 cm depth intervals for sediments of Units 2, 3 and 4 (see results for definition), following the procedures in Rothwell and Rack (2006). The sediment was sieved to remove particles larger than 2 mm before the sample was dispersed in a 1 l mixing chamber by shaking it for 24 h. The dispersed sediment was circulated through a Malvern Mastersizer 3000 for 120 s over which time 12 measurements are taken and then averaged to obtain the grain-size distribution.

Geotechnical analyses

Water content and fall cone measurements were carried out at 10 cm intervals (BSI 1990; BSI 2004). Measurements of water content could be used as a

first-order approximation of the sediment's shear strength and compressibility (i.e. higher water content is related to low shear strength and high compressibility). An 80 g 30° fall cone was used on the split cores, regardless of the grain size and whether the tested material was considered to be saturated or not. The undrained shear strength was calculated from the fall cone measurements assuming all tests were carried out on saturated clays. Subsamples were taken for subsequent direct shear and oedometric tests.

Static, drained shear test. Direct shear experiments were carried out to compare the drained shear strength of prominent layers, identified from downcore logging, grain-size distribution and standard geotechnical data. Cylindrical, undisturbed samples (*c.* 5 cm², 2.5 cm height) of intact samples were placed in the shear apparatus and consolidated via a vertical ram to *in situ* normal stress (σ_n). The sample was consolidated until the sample height was constant (or min. 24 h), so that the sample is assumed to be fully drained and the applied σ_n is approximately equal to the effective normal stress (σ'_n). The effective normal stress is the difference between the normal stress and the pore water pressure, u ($\sigma'_n = \sigma_n - u$; Terzaghi 1925). Shearing occurs on a predefined plane, perpendicular to the vertical ram that exerts the normal stress. The shear displacement for each experiment was 9.5 mm at a shear rate of 0.008 mm min⁻¹. This shear rate was slow enough to allow constant drainage during shearing (Deutsches

Institut für Normung 2002). Samples were taken from around 7 m core depth, which corresponds to around 18 m below seafloor (assuming around 10 m of sediment was removed during the failure). The samples were sheared at a normal stress of 170 kPa, simulating the effective hydrostatic vertical over-burden stress (σ'_{v0}) acting at around 18 m below sea-floor (m bsf) assuming an average sediment effective unit weight (γ') of 9.5 kN m^{-3}.

Oedometer test. One-dimension consolidation tests were performed on selected undisturbed core samples (*c.* 20 cm^2, 1.9 cm height) in order to measure and compare their permeability and consolidation parameters. The measured initial porosity (*n*), coefficient of compression (c_v) and permeability (*k*) can be used to make assumptions regarding the sediments' potential to build excess pore pressure. Incremental loading and unloading of 1 kPa to 7100 kPa stress were applied onto the sediment and the resulting displacement (change in volume) was measured. Each load was applied gradually and left until the displacement stabilized or primary consolidation was completed. Consolidation and permeability parameters were calculated from the settlement characteristics of the sediment using standard equations (Powrie 2013).

Data analysis

Physical and geochemical properties were compared using non-parametric tests that compare two unpaired groups of data and compute *p*-values testing the null hypothesis of two groups having the same distribution. The data were analysed for the discrepancy between the mean ranks of two groups (Mann–Whitney test) and for their varying cumulative distribution (Kolmogorov–Smirnov test) (Sheskin 2011). The significance level for both tests was set to 0.05 (Fisher 1926).

Results

Piston core 64PE391-04 was obtained about 750 m down-slope from where the sediment ramped up the failure plane on to the seabed (failure Stage 1, Wilson *et al.* 2004; Fig. 2c). The deep-tow boomer reflection seismic data indicate that the core penetrated the pre-landslide sediments, including those stratigraphically equivalent to the failure plane of the slide. Based on the newly obtained data, we identify five main lithological units within the sediment core, which we now characterize using results from visual sediment core logging, particle size distribution, X-ray scanning, and continuous physical properties (MSCL) and geochemical (micro-XRF) measurements (see summary in Figs 3 & 4). In addition, we present a geotechnical characterization of the

recovered sediment based on water content and fall cone analyses, as well as direct shear (DS) and oedometer tests.

Visual sedimentary logging and grain-size analyses indicate that the general lithology is bioturbated silty clay to clayey silt with a number of sandy silt and silty sand layers, consistent with previous analyses of sediment cores from the area (Madhusudhan *et al.* 2017). Sandy layers are found only in the upper part of the core (above 7.3 m depth). The lithology in the lower part of the core is generally homogeneous with an absence of sand.

Multi-Sensor Core Logger (MSCL) data

Down-core logging data show an abrupt and distinct change in physical properties at around 7.3 m depth, as well as more subtle variations that enabled demarcation of the five sediment units (Fig. 3; Table 2). Unit 1 is largely indiscernible from Unit 2 based on physical properties, but does have much lower magnetic susceptibility. The sediments above the abrupt contact at 7.3 m (Units 2 and 3) are generally characterized by high relative P-wave velocities, gamma-ray densities, electrical resistivity, and low relative values of fractional porosity (on average under 0.5). Unit 3 shows the highest electrical resistivity and gamma-ray densities in the core; hence, it is demarcated as an individual unit, rather than being subsumed within Unit 2. In the sediments immediately below 7.3 m (Unit 4), the most marked step in physical properties is observed, including a reduction in gamma-ray density from 2.0 to 1.7 g cm^{-3}, and an increase in fractional porosity from approximately 0.45 to >0.55. Such a marked change was not observed in the magnetic susceptibility this side of the contact either; however, the signal is generally more erratic above and less variable below (Fig. 3). Below the contact at 7.3 m, P-wave velocity, gamma-ray density and electrical resistivity gradually increase down-core (inversely mirroring a steady decrease in fractional porosity) until the start of Unit 5, which is marked by a sharp increase in magnetic susceptibility (from <70 to >165 m^3 kg^{-1}), and a subtle increase in average P-wave velocity and gamma-ray density (Fig. 3).

Micro-X-ray fluorescence (XRF) data

Distinct changes in geochemistry are also observed from the micro-XRF analysis between the sediment units (Figs 3 & 5), which correspond to very similar depths (± 0.3 m) where physical property changes are noted. The first-order observations are of: (i) a step in Fe/K, Ca/Fe and Ca/Sr elemental ratios between 7.1 and 7.3 m (i.e. straddling Unit 2/3/4 contacts); and (ii) a switch from more variable (noisy) elemental ratios above 7.1–7.3 m (Units 2
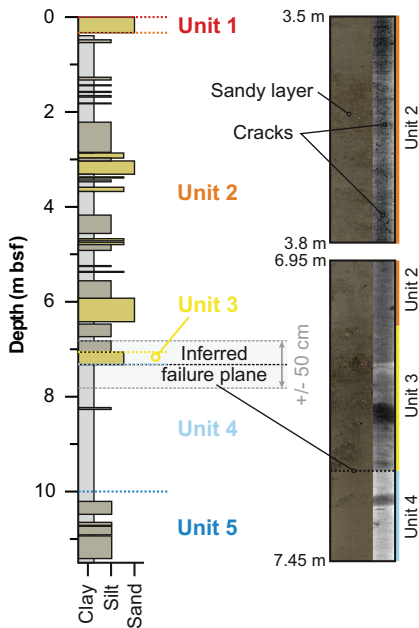
Fig. 4. Inferred location of the main failure plane based on down-core logging and deep-tow boomer reflection seismic data. Units 1–5 are outlined. Vertical error in the failure plane delineation, resulting from the vertical resolution of the seismic data is indicated by grey lines (± 50 cm from the inferred failure plane). Core images and X-radiographs from the inferred failure plane and cracks in Unit 2 are also shown.

and 3), with centimetre-scale variations in geochemical composition, to less noisy ratios below (Unit 4). Below Unit 4, variations in elemental ratios are also observed, supporting the demarcation of Unit 5. Cross-plotting of the elemental ratios (Fig. 6) supports the demarcation of the five identified sediment units, as well as illustrating the range in variability between each unit (e.g. a large spread of values in Unit 2, compared to Unit 4).

Grain-size distribution

Figure 7 summarizes grain-size distribution data for core section 64PE391-04-D (6.5–7.7 m depth), which include sediments from Units 2, 3 and 4. The data illustrate the change in composition at around 7.3 m depth. Unit 4 (below 7.3 m depth) is characterized by a higher silt content in comparison to overlying sediments. Unit 3 is recognized as a sandy silt layer, and the sampled sediments of Unit 2 show a switch from sandy silt to clayey silt, which supports the distinct changes in lithology seen in the visual core log.

Geotechnical data

A distinct change in water content can be observed, which increases from around 30% to over 60% at 7.3 m depth (i.e. at the contact between Units 3 and 4; Fig. 3). Unit 1 has a slightly higher water content than Unit 2 (more or less constant 30%). Units 4 and 5 are characterized by decreasing water content. A distinct change in the undrained shear strength is not observed, although the scatter is greater in the upper part of the core (Units 2 and 3). Individual outliers (>100 kPa) are related to dropstones or mud clasts.

A summary of the key sample parameters and test results of the direct shear and oedometer tests are given in Table 3. The peak drained shear strength of Units 3 and 4 are shown in Figure 3 (indicated by red crosses). It can be seen that Unit 3 encompasses a higher peak shear strength (173 kPa) than Unit 4 (109 kPa). Typical porosity (n) v. applied normal stress (σ_n) is shown in Figure 8. It is apparent that porosity decreases with increasing normal stress and increases slightly during the rebound phase. Unit 3 has a lower initial porosity, and higher permeability (k) and compressibility (c_v) than Unit 4.

Discussion

The recovered slope sediment obtained from core 64PE391-04 is characterized by a distinct step change in both physical and geochemical properties between around 7.1 and 7.3 m depth, as well as a distinct high-density contrast at that depth that was recorded by X-ray imaging (Figs 3 & 4). These transitions are related to an abrupt change in lithology from a thick relatively homogeneous clayey silt, silty clay unit (Unit 4; Figs 3 & 5) to an overlying 25 cm-thick sandy silt layer (Unit 3; Figs 3 & 5). The depth of this distinct change matches well with the seismostratigraphic horizon that is equivalent to the main failure plane outlined in the deep-tow boomer reflection seismic data (assuming a seismic velocity of 1600 m s^{-1}; Wilson *et al.* 2004), which is supported by the available MSCL data.

The sediment above this distinct interface is characterized by slightly higher P-wave velocities and gamma-ray densities, as well as a lower fractional porosity than would be expected for continental slope sediments (Fig. 3; Hamilton 1970). Small cracks were recorded by X-ray imaging, but are limited to parts of Unit 2 (Fig. 4). These observations could be related to a slight compaction of the sediment, for example, due to compression by the partially confined landslide debris above the sediment ramp (Fig. 2c; e.g. Frey-Martínez *et al.* 2006; Princi-paud *et al.* 2015; Brooks *et al.* 2018), or to the around

Table 2. *Summary of sediment core's sedimentological, geophysical and geochemical characteristics*

| Unit and depth range (m)	General sedimentological description	MSCL characterization	XRF characterization	Possible deposit interpretation
Unit 1 (0–0.33)	Muddy sand	Lower magnetic susceptibility, no distinct trends in other geophysical properties	>Ca/Fe; No distinct Ca/Sr or Fe/K trend	Recent current reworked deposits
Unit 2 (0.33–7.11)	Stratified unit, consisting of bioturbated clayey silt to silty clay and sandy silt to silty sand layers; drop stones in the upper part of the unit	Strong variations in P-wave velocity, gamma-ray density, fractional porosity and magnetic susceptibility; down-core increase in P-wave velocity and gamma-ray density, and decrease in fractional porosity	Strong variations especially in Ca/Fe	Post-glacial deposits, with variable pulses of sediment flux including melt-water plumes
Unit 3 (7.11– 7.32)	Sandy silt layer; mud clasts	High P-wave velocity and electrical resistivity	Increase in Ca/Sr; decrease in Ca/Fe; distinct increase in Fe/K	Sandy contourite, reworked from immediate post-glacial meltwater-derived sediments
Unit 4 (7.32–10.00)	Relatively homogeneous bioturbated silty clay to clayey silt; drop stones throughout the unit	Distinct and abrupt decrease in P-wave velocity, gamma-ray density and electrical resistivity, and increase in fractional porosity at contact with Unit 3; less variation in magnetic susceptibility	Relatively constant element ratios; higher average Ca/Sr (and peak); lower average Ca/Fe; higher average Fe/K	Steady glaciomarine deposition
Unit 5 (10.00–end)	Clayey silt to sandy silt	Distinct and abrupt increase in magnetic susceptibility at contact with Unit 4; slight increase in P-wave velocity and gamma-ray density	Slightly variations in Ca/Sr; increasing Ca/Fe; distinct increase in Fe/K;	Steady interstadial deposition

Submarine slope failure in contourites
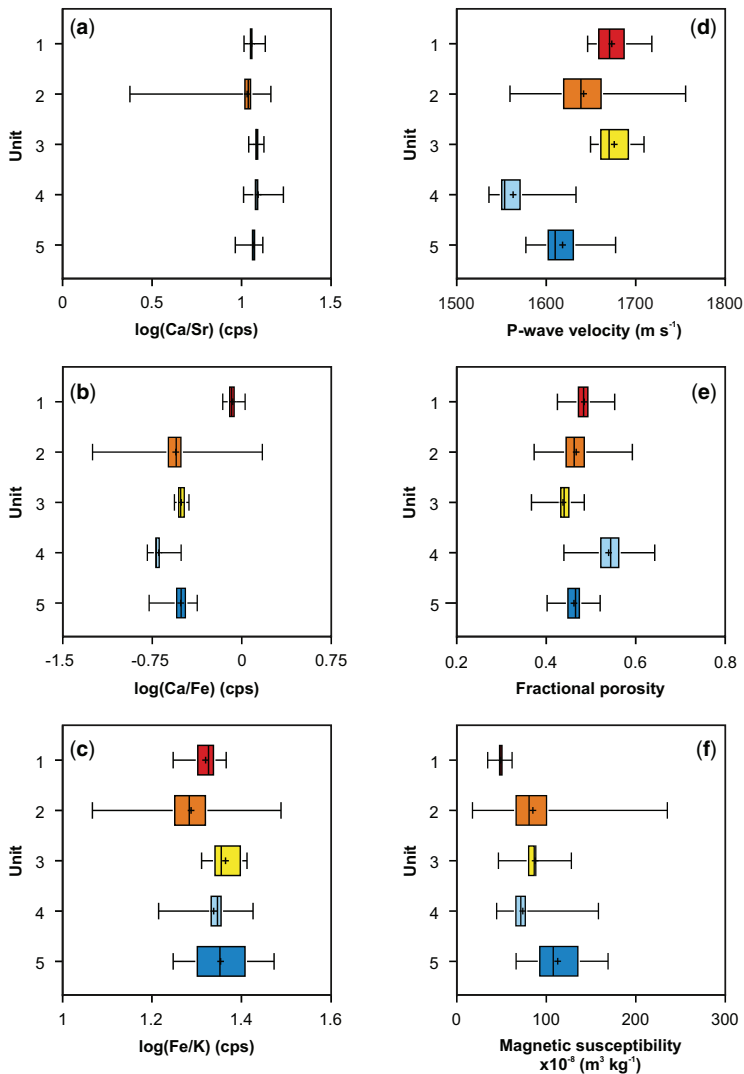
Fig. 5. Box-whisker plots showing the variation in element ratios (**a**) Ca/Sr, (**b**) Ca/Fe and (**c**) Fe/K, and (**d–f**) physical properties between Units 1–5. The lines of the box indicate the upper and lower quartiles and the median, lines extending parallel from the boxes indicate the maximum and minimum values and the cross illustrates the mean value.

10 m missing sediment sequence at the 64PE391-04 core location (Fig. 2), whose removal could have disturbed the slope sediments. The potential deformation, however, is not resolved in the seismic data, and the distinct change at around 7.1–7.3 m depth is not limited to the physical properties, but is also noted in the geochemical properties. We therefore infer that although the sediment might have been slightly deformed, it probably did not move (no sliding motion) and the stratigraphy was not altered.

Lithological contrasts appear to play a key role in dictating the location of the failure plane

Wilson *et al.* (2004) previously suggested that the AFEN Slide could have initiated along a sandy contouritic layer embedded within the slope stratigraphy, but were unable to sample deep enough to show its occurrence. Our deeper core now shows that this hypothesis may be plausible, given the presence of Unit 3. Although this unit was not identified
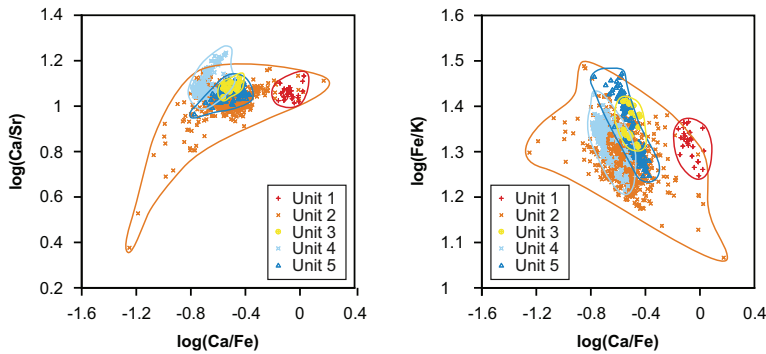
Fig. 6. ITRAX XRF composition of individual subunits compared as cross plots. Red crosses, Unit 1; orange crosses, Unit 2; yellow circles, Unit 3; light blue stars, Unit 4; dark blue triangles, Unit 5.

as a contourite in the seismic data (Fig. 2c, Wilson *et al.* 2004), we interpret it as a sheeted sandy contourite drift. This assumption is considered reasonable as the vertical resolution of the seismic data (0.5 m; Wilson *et al.* 2005) might be too low to register this 25 cm-thick layer. Furthermore, we also show that there is much greater lithological heterogeneity (based on physical properties and geochemistry) within these sheeted drifts than has been previously documented, aside from simply variations in grain size. Without detailed geochemical and physical properties data, this abrupt lithological change would not have been identified.

Abrupt lithological changes (such as between Units 3 and 4) may instead play a key role in defining the location of the failure plane. Unfortunately, the vertical resolution of the existing seismic data does not enable us to categorically determine whether the failure plane should correspond to the contact of Units 3/4 or 2/3. Although varying the assumed seismic velocity within reasonable ranges for sediments only results in a vertical offset of 0.5 m, the failure plane falls within the depth window that includes the interfaces between Units 2/3 and 3/4 (Fig. 4). Wilson *et al.* (2004) implicated sandy contouritic sediments as potential 'weak layers' (i.e. Units 2/3 scenario) because of their potential to generate excess pore pressures when bound by an overlying lower permeability unit. This is a reasonable suggestion; however, the fractional porosity data indicate that the sand-rich Unit 3 instead features slightly lower porosity than the overlying sediments, while the underlying mud-rich sediments (Unit 4) have an even higher porosity. This observation is supported by water content data, which show the highest values in the mud-rich Unit 4 and abruptly
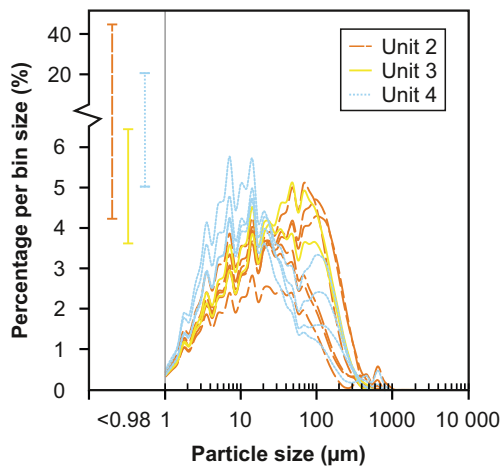

Fig. 7. Particle-size distribution data illustrated as percentage per bin. The data are binned as frequency per 1/4 phi unit. Particle size <0.98 is given as percentage range per Unit.

Table 3. *Key sample parameters and results from direct shear and oedometer tests*

Sample	Unit 3	Unit 4
LL (%)	26.5	56.1
PL (%)	–	25
γ' (kN m^{-3})	9.5	9.5
σ'_n (kPa)	170	170
τ_{peak} (kPa)	173	109
n	0.43	0.55
c_v (m^2 s^{-1})	5.2×10^{-4}	7.6×10^{-5}
k (m s^{-1})	4.3×10^{-7}	7.8×10^{-8}

LL, liquid limit; PL, plastic limit; γ', effective unit weight; σ'_n, effective normal stress; τ_{peak}, peak shear strength; n, porosity; c_v, compressibility; k, permeability.
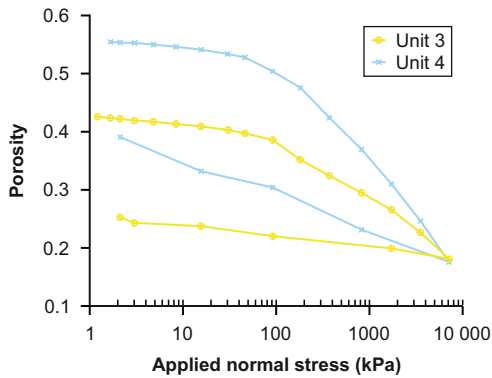
Fig. 8. Porosity (*n*) v. applied normal stress (σ_n) curves from one-dimensional consolidation tests.

decrease at the interface to Unit 3. Oedometer tests carried out on undisturbed samples from Units 3 and 4 reveal a higher initial porosity and lower compressibility of Unit 4. This relationship is in contrast to an established empirical relationship between coarser grain size and greater porosity (or larger pore size; Ren and Santamarina 2018). This apparent contradiction is explained by the presence of detrital clay that fills in pore spaces between sand grains (Unit 3), whereas the relatively open structure of the underlying muddier deposits (Unit 4) explains their higher relative porosity (Marion *et al.* 1992; Revil and Cathles III 1999). In contrast to porosity, however, permeability is found to be higher in the sand-rich sediments (Unit 3; Table 3). Considering the higher permeability and compressibility of Unit 3, it is possible for excess pore pressure to accumulate within the sandy contouritic sediments (e.g. during an earthquake). Although this observation would support the 'weak layer' hypothesis, it has to be noted that the water content is actually higher in Unit 4 and abruptly drops at the interface with Unit 3, instead of increasing within the layer.

Another noticeable observation is the difference in shear strength between Units 3 and 4. Both drained and undrained shear strength are lower in the mud-rich Unit 4, which can be related to the higher water content and the lack of sandy material within the unit. Taking all these observations into account, we suggest that it is possible that a failure plane could generate at an interface where sand overlies finer-grained cohesive sediments. The high water content and lower shear strength of the fine-grained material could allow the overlying sediment to slide on top of it. We are unable to be more absolute on the failure depth, but we have demonstrated that variability in sheeted drifts can also include abrupt whole-scale changes in sediment properties, as well as the presence of thin coarser units, which

have traditionally been invoked to explain bedding-parallel failures in contourite sheeted drifts (Laberg and Camerlenghi 2008). Such variability may not necessarily be expected based on the available seismic data alone.

Climate change is a likely control on creating failure-prone lithological contrasts

Down-core changes in Ca/Sr ratios have been successfully related to variations in sea-level and water temperature (through integration with oxygen isotope curves and biostratigraphy), wherein high Ca/Sr ratios are indicative of ice-rafted debris and changes from colder to warmer conditions (e.g. Smith *et al.* 1979; Thomson *et al.* 2004; Hodell *et al.* 2008). High Fe/K ratios and low Ca/Fe, on the other hand, have been related to colder periods (Kuijpers *et al.* 2003; Perez *et al.* 2016). The increased Ca/Sr ratio above 7.6 m depth could therefore indicate a stronger meltwater flux, carrying ice-rafted debris into the channel, while the changes in Fe/K and Ca/Fe ratios at 7.1–7.3 m are also interpreted to indicate a switch from cold conditions (Unit 4) to warmer conditions (Units 2/3). This switch was coincident with a transition from finer-grained, stable sedimentation to a more variable regime with pulsed influxes of coarser material. Given the existing knowledge about the timing of the AFEN Slide (Unit 1 should post-date 2.8–5.8 ka BP, while the pre-failure sediments must be older than 16 ka BP; Wilson *et al.* 2004), this transition fits within a time window that includes the switch from the LGM (18 ka BP) to post-glacial conditions. Glacial conditions would have seen sediment largely locked up in ice sheets, while the melt-out during the immediate postglacial window involved pulses of fine- and coarser-grained sediment. The nearby Faroe–Shetland Channel is the main oceanic gateway between the North Atlantic and the Norwegian Sea (Broecker and Denton 1990; Rahmstorf 2002), where a direct relation exists between ocean circulation and climate. Rapid changes in the exchange of water masses between the NE Atlantic and the Norwegian Sea occurred following the LGM at 18 ka BP (Rasmussen *et al.* 2002), which would have compounded the abruptness of a switch in sediment transfer. We therefore suggest that the abrupt change in physical properties and geochemistry may relate to this climatic transition.

Previous studies have investigated the role of climate change on submarine landslides, primarily focusing on their timing. A number of early studies suggested that submarine landslides, particularly in higher latitudes, may be more likely during sea-level lowstands. Recent work, however, has suggested

that there is no clear statistical relationship or at least that there are too few observations to be confident (e.g. Maslin *et al.* 2004; Brothers *et al.* 2013; Urlaub *et al.* 2013, 2014; Pope *et al.* 2015). Indeed, recent work has shown that such margins may feature many more late Holocene submarine landslides than previously thought (Normandeau *et al.* 2019). Proving a clear link between submarine landslides and sea-level or climate change is most likely complicated by a range of factors, including time lags in offshore sediment transport, residence times of excess pore pressures following periods of rapid sediment accumulation, local sea-level changes (e.g. isostatic rebound following glaciations) and other factors (Masson *et al.* 2006; Urgeles and Camerlenghi 2013; Talling *et al.* 2014). Whether climate change has played any role in the timing of the slope failures at AFEN remains unclear; however, it may have played a key role in one aspect: the location of the failure plane. Our data indicate that the slope failure most likely initiated along a distinct lithological interface that is interpreted to relate to a switch in depositional regime: from cold and uniform to warm and variable depositional conditions. The close connection between thermohaline circulation, sea-level and temperature, and sediment supply in this region may explain why the switch in deposition was so rapid.

Broader implications for slope instability in contourites at climatically influenced ocean gateways

The origin of distinct lithological interfaces may arise in a variety of ways, and may be very common in contouritic sediments near ocean gateways where climatic changes may affect bottom current intensity (and thus control the grain-size that is transported; Faugères and Mulder 2011), as well as the type of sediment that is distributed by bottom currents (e.g. terrestrial and biogenic fluxes may vary during different climatic windows; Faugères *et al.* 1993; Maldonado *et al.* 2005). Such effects can be felt at a variety of latitudes, ranging from tropical to polar settings (e.g. Kuijpers *et al.* 2001; Principaud *et al.* 2015; Elger *et al.* 2017). Climate may play a key role in dictating the location of potential failure planes. While many previous studies have invoked dominantly geometric controls on slope failure in contourite drifts, our study contributes to a growing literature base that indicates that lithological interfaces may explain the strong affinity of contourite deposits to slope instability. We posit that in low-angle, sheeted contourite drifts, such as AFEN, it is such material interfaces that are most important for preconditioning slopes to failure.

Conclusions

The integration of physical properties and geochemical core-log data, grain-size distribution, and geotechnical data indicate that the AFEN Slide initiated along a distinct lithological interface within the slope stratigraphy, which matches the depth of the failure plane obtained from seismic data. This lithological interface correlates with the base of a 25 cm sandy contourite layer, overlying a thick, relatively homogeneous silty clay unit. Based on this high-resolution multi-proxy analysis, it was possible to resolve small-scale material changes within the slope stratigraphy, which cannot be distinguished from seismic data alone (owing to the limited vertical resolution of 0.5 m). Integrating the core analyses with our knowledge about the current regime prevailing in the Faroe–Shetland Channel for the last 18 ka, it seems that climate change might precondition the location of failure initiation. This highlights the fact that in order to understand submarine landslide hazard, it is necessary to include information from all different scales, ranging from the small-scale high-resolution analysis of core material to the understanding of the regional oceanographic setting.

Author contributions RG: conceptualization (equal), data curation (supporting), investigation (equal), methodology (equal), validation (equal), visualization (lead), writing – original draft (lead), writing – review and editing (lead); **MAC**: conceptualization (equal),

References

Ai, F., Strasser, M., Preu, B., Hanebuth, T.J.J., Krastel, S. and Kopf, A. 2014. New constraints on oceanographic vs. seismic control on submarine landslides initiation: a geotechnical approach off Uruguay and northern Argentina. *Geo-Marine Letters*, **34**: 399–417, https://doi.org/10.1007/s00367-014-0373-3

Andersen, M.S., Nielsen, T., Sørensen, A.B., Boldreel, L.O. and Kuijpers, A. 2000. Cenozoic sediment distribution and tectonic movements in the Faroe region. *Global and Planetary Change*, **24**, 239–259, https://doi.org/10.1016/S0921-8181(00)00011-4

Baeten, N.J., Laberg, J.S. *et al.* 2013. Morphology and origin of smaller-scale mass movements on the continental slope off northern Norway. *Geomorphology*, **187**, 122–134, https://doi.org/10.1016/j.geomorph.2013.01.008

Baeten, N.J., Laberg, J.S. *et al.* 2014. Origin of shallow submarine mass movements and their glide planes – Sedimentological and geotechnical analyses from the continental slope of northern Norway. *Journal of Geophysical Research: Earth Surface*, **119**, 2335–2360, https://doi.org/10.1002/2013JF003068

Blindheim, J. 1990. Arctic intermediate water in the Norwegian Sea. *Deep-Sea Research*, **37**, 1475–1489, https://doi.org/10.1016/0198-0149(90)90138-L

Bonnin, J., van Raaphorst, W., Brummer, G.-J., van Haren, H. and Malschaert, H. 2002. Intense mid-slope resuspension of particulate matter in the Faeroe–Shetland Channel: short-term deployment of near-bottom sediment traps. *Deep-Sea Research I*, **49**, 1485–1505, https://doi.org/10.1016/S0967-0637(02)00030-4

Broecker, W.S. and Denton, G.H. 1990. The role of ocean–atmosphere reorganizations in glacial cycles. *Quaternary Science Reviews*, **9**, 305–341, https://doi.org/10.1016/0277-3791(90)90026-7

Brooks, H.L., Hodgson, D.M., Brunt, R.L., Peakall, J. and Flint, S.S. 2018. Exhumed lateral margins and increasing flow confinement of a submarine landslide complex. *Sedimentology*, **65**, 1067–1069, https://doi.org/10.1111/sed.12415

Brothers, D.S., Luttrell, K.M. and Chaytor, J.D., 2013. Sea-level–induced seismicity and submarine landslide occurrence. *Geology*, **41**, 979–982, https://doi.org/10.1130/G34410.1

Bryn, P., Berg, K., Forsberg, C.F., Solheim, A. and Kvalstad, T.J. 2005a. Explaining the Storegga Slide. *Marine and Petroleum Geology*, **22**, 11–19, https://doi.org/10.1016/j.marpetgeo.2004.12.003

Bryn, P., Berg, K., Stoker, M.S., Haflidason, H. and Solheim, A. 2005b. Contourites and their relevance for mass wasting along the Mid-Norwegian Margin. *Marine and Petroleum Geology*, **22**, 85–96, https://doi.org/10.1016/j.marpetgeo.2004.10.012

BSI 1990. Methods of test for soils for civil engineering purposes – Part 2: classification tests. *In*: *British Standard BS 1377–2*. British Standards Institution, London.

BSI 2004. Geotechnical investigation and testing – laboratory testing of soils. Part 6: fall cone tests. *In*: *DD CEN ISO/TS 17892-6*. British Standards Institution, London.

Casas, D., Chiocci, F., Casalbore, D., Ercilla, G. and De Urbina, J.O. 2016. Magnitude-frequency distribution of submarine landslides in the Gioia Basin (southern Tyrrhenian Sea). *Geo-Marine Letters*, **36**, 405–414, https://doi.org/10.1007/s00367-016-0458-2

Chaytor, J.D., Uri, S., Solow, A.R. and Andrews, B.D. 2009. Size distribution of submarine landslides along the US Atlantic margin. *Marine Geology*, **264**, 16–27, https://doi.org/10.1016/j.margeo.2008.08.007

Clare, M.A., Chaytor, J. *et al.* 2018. A consistent global approach for the morphometric characterization of subaqueous landslides. *Geological Society, London, Special Publications*, **477**, https://doi.org/10.1144/SP477.15

Croudace, I.W. and Rothwell, R.G. (eds) 2015. *Micro-XRF Studies of Sediment Cores. Applications of a Non-Destructive Tool for the Environmental Sciences*. Springer, Dordrecht.

Croudace, I.W., Rindby, A. and Rothwell, R.G. 2006. ITRAX: description and evaluation of a new multifunction X-ray core scanner. *Geological Society, London, Special Publications*, **267**, 51–63, https://doi.org/10.1144/GSL.SP.2006.267.01.04

Dahlgren, K.I.T., Vorren, T.O. and Laberg, J.S. 2002. Late Quaternary glacial development of the mid-Norwegian margin – 65 to 68°N. *Marine and Petroleum Geology*, **19**, 1089–1113, https://doi.org/10.1016/S0264-8172(03)00004-7

Davies, R.J., Cartwright, J.A., Pike, J. and Line, C. 2001. Early Oligocene initiation of North Atlantic deep water formation. *Nature*, **410**, 917–920, https://doi.org/10.1038/35073551

Dean, K., McLachlan, K. and Chambers, A. 1999. Rifting and the development of the Faeroe-Shetland Basin. *Geological Society, London, Petroleum Geology Conference Series*, **5**, 533–544, https://doi.org/10.1144/0050533

Deutsches Institut für Normung 2002. Baugrund, Untersuchung von Bodenproben – Bestimmung der Scherfestigkeit. *In*: *DIN-Norm 18137- 3*. Beuth, Berlin.

Elger, J., Berndt, C., Krastel, S., Piper, D.J.W., Gross, F. and Geissler, W.H. 2017. Chronology of the Fram Slide Complex offshore NW Svalbard and its implications for local and regional slope stability. *Marine Geology*, **393**, 141–155, https://doi.org/10.1016/j.margeo.2016.11.003

Ercilla, G., Juan, C. *et al.* 2016. Significance of bottom currents in deep-sea morphodynamics: an example from

the Alboran Sea. *Marine Geology*, **378**, 157–170, https://doi.org/10.1016/j.margeo.2015.09.007

Evans, D., Harrison, Z. *et al.* 2005. Paleoslides and other mass failures of Pliocene to Pleistocene age along the Atlantic continental margin of NW Europe. *Marine and Petroleum Geology*, **22**, 1131–1148, https://doi.org/10.1016/j.marpetgeo.2005.01.010

Faugères, J.-C. and Mulder, T. 2011. Contour currents and contourite drifts. *Developments in Sedimentology*, **63**, 149–214, https://doi.org/10.1016/B978-0-444-53000-4.00003-2

Faugères, J.-C. and Stow, D.A.V. 2008. Contourite drifts: nature, evolution and controls. *Developments in Sedimentology*, **60**, 259–288, https://doi.org/10.1016/S0070-4571(08)10014-0

Faugères, J.-C., Mézerais, M.L. and Stow, D.A.V. 1993. Contourite drift types and their distribution in the North and South Atlantic Ocean basins. *Sedimentary Geology*, **82**, 189–203, https://doi.org/10.1016/0037-0738(93)90121-K

Faugères, J.-C., Stow, D.A.V., Imbert, P. and Viana, A. 1999. Seismic features diagnostic of contourite drifts. *Marine Geology*, **162**, 1–38, https://doi.org/10.1016/S0025-3227(99)00068-7

Fisher, R.A. 1926. The arrangement of field experiments. *Journal of the Ministry of Agriculture of Great Britain*, **33**, 503–513.

Frey-Martínez, J., Cartwright, J. and James, D. 2006. Frontally confined versus frontally emergent submarine landslides: a 3D seismic characterisation. *Marine and Petroleum Geology*, **23**, 585–604, https://doi.org/10.1016/j.marpetgeo.2006.04.002

Georgiopoulou, A., Shannon, P.M., Sacchetti, F., Haughton, P.D.W. and Benetti, S. 2013. Basement-controlled multiple slope collapses, Rockall Bank Slide Complex, NE Atlantic. *Marine Geology*, **336**, 198–214, https://doi.org/10.1016/j.margeo.2012.12.003

Georgiopoulou, A., Krastel, S. *et al.* 2019. On the timing and nature of the multiple phase of slope instability on Eastern Rockall Bank, Northeast Atlantic. *Geochemistry, Geophysics, Geosystems*, **20**, 594–613, https://doi.org/10.1029/2018GC007674

Gunn, D.E. and Best, A.I. 1998. A new automated non-destructive system for high resolution multi-sensor core logging of open sediment cores. *Geo-Marine Letters*, **18**, 70–77, https://doi.org/10.1007/s003670050054

Haflidason, H., Lien, R., Sejrup, H.P., Forsberg, C.F. and Bryn, P. 2005. The dating and morphometry of the Storegga Slide. *Marine and Petroleum Geology*, **22**, 123–136, https://doi.org/10.1016/j.marpetgeo.2004.10.008

Hamilton, E.L. 1970. Sound velocity and related properties of marine sediments, North Pacific. *Journal of Geophysical Research*, **75**, 4423–4446, https://doi.org/10.1029/JB075i023p04423

Henkel, S., Strasser, M. *et al.* 2011. An interdisciplinary investigation of a recent submarine mass transport deposit at the continental margin off Uruguay. *Geochemistry, Geophysics, Geosystems*, **12**, Q08009, https://doi.org/10.1029/2011GC003669

Hepp, D.A., Mörz, T. and Grützner, J. 2006. Pliocene glacial cyclicity in a deep-sea sediment drift (Antarctic Peninsula Pacific Margin). *Paleogeography,*

Paleoclimatology, Paleoecology, **231**, 181–198, https://doi.org/10.1016/j.palaeo.2005.07.030

Hernández-Molina, F.J., Llave, E. and Stow, D.A.V. 2008. Continental slope contourites. *Developments in Sedimentology*, **60**, 379–408, https://doi.org/10.1016/S0070-4571(08)10019-X

Hernández-Molina, F.J., Paterlini, M., Violante, R., Marshall, P., de Isasi, M., Somoza, L. and Rebesco, M. 2009. Contourite depositional system on the Argentine Slope: an exceptional record of the influence of Antarctic water masses. *Geology*, **37**, 507–510, https://doi.org/10.1130/G25578A.1

Hernández-Molina, F.J., Soto, M. *et al.* 2016. A contourite depositional system along the Uruguayan continental margin: sedimentary, oceanographic and paleoceanographic implications. *Marine Geology*, **378**, 333–349, https://doi.org/10.1016/j.margeo.2015.10.008

Hodell, D.A., Channell, J.E.T., Curtis, J.H., Romero, O.E. and Röhl, U. 2008. Onset of "Hudson Strait" Heinrich events in the eastern North Atlantic at the end of the middle Pleistocene transition ($\sim$640 ka)?. *Paleoceanography*, **23**, PA4218, https://doi.org/10.1029/2008PA001591

Hohbein, M. and Cartwright, J. 2006. 3D seismic analysis of the West Shetland Drift system: implications for Late Neogene paleoceanography of the NE Atlantic. *Marine Geology*, **230**, 1–20, https://doi.org/10.1016/j.margeo.2006.03.009

Hübscher, C., Betzler, C. and Reiche, S. 2016. Seismo-stratigraphic evidences of deep base level control on middle to late Pleistocene drift evolution and mass wasting along southern Levant continental slope (Eastern Mediterranean). *Marine and Petroleum Geology*, **77**, 526–534, https://doi.org/10.1016/j.marpetgeo.2016.07.008

Hühnerbach, V., Masson, D.G. and partners of the COSTA-Project 2004. Landslides in the North Atlantic and its adjacent seas: an analysis of their morphology, setting and behaviour. *Marine Geology*, **213**, 343–362, https://doi.org/10.1016/j.margeo.2004.10.013

Iwai, M., Acton, G.D., Lazarus, D., Osterman, L.E. and Williams, T. 2002. Magnetobiochronologic synthesis of ODP Leg 178 rise sediments from the Pacific sector of the Southern Ocean: sites 1095, 1096, and 1101. *In*: Barker, P.F., Camerlenghi, A., Acton, G.D. and Ramsay, A.T.S. (eds) *Proceedings of ODP, Scientific Results*, **178**. Ocean Drilling Program, College Station, TX, 1–40.

Jackson, P.D., Gunn, D.A. and Long, D. 2004. Predicting variability in the stability of slope sediments due to earthquake ground motion in the AFEN area of the western UK continental shelf. *Marine Geology*, **213**, 363–378, https://doi.org/10.1016/j.margeo.2004.10.014

Johnson, H., Ritchie, J.D., Hitchen, K., Mcinroy, D.B. and Kimbell, G.S. 2005. Aspects of the Cenozoic deformational history of the Northeast Faroe–Shetland Basin, Wyville-Thomson Ridge and Hatton Bank areas. *Geological Society, London, Petroleum Geology Conference Series*, **6**, 993–1007, https://doi.org/10.1144/0060993

Katz, O., Reuven, E. and Aharonov, E. 2015. Submarine landslides and fault scarps along the eastern Mediterranean Israeli continental-slope. *Marine Geology*,

369, 100–115, https://doi.org/10.1016/j.margeo.2015.08.006

Knutz, P.C. and Cartwright,. 2004. 3D anatomy of late Neogene contourite drifts and associated mass flows in the Faroe–Shetland Basin. *Geological Society, London, Memoirs*, **29**, 63–71, https://doi.org/10.1144/GSL.MEM.2004.029.01.07

Krastel, S., Wefer, G. *et al*. 2011. Sediment dynamics and geohazards off Uruguay and the de la Plata River region (northern Argentina and Uruguay). *Geo-Marine Letters*, **31**, 271–283, https://doi.org/10.1007/s00367-011-0232-4

Kuhlmann, J., Asioli, A., Trincardi, F., Klügel, A. and Huhn, K. 2017. Landslide frequency and failure mechanisms at NE Gela Basin (Strait of Sicily). *Journal of Geophysical Research: Earth Surface*, **122**, 2223–2243, https://doi.org/10.1002/2017JF004251

Kuijpers, A., Nielsen, T., Akhmetzhanov, A., de Haas, H., Kenyon, N.H. and van Weering, T.C.E. 2001. Late Quaternary slope instability on the Faeroe margin: mass flow features and timing of events. *Geo-Marine Letters*, **20**, 149–159, https://doi.org/10.1007/s003670000053

Kuijpers, A., Troelstra, S.R. *et al*. 2003. Late Quaternary sedimentary processes and ocean circulation changes at the Southeast Greenland margin. *Marine Geology*, **195**, 109–129, https://doi.org/10.1016/S0025-3227(02)00684-9

Kvalstad, T.J., Andresen, L., Forsberg, C.F., Berg, K., Bryn, P. and Wangen, M. 2005. The Storegga slide: evolution of triggering sources and slide mechanics. *Marine and Petroleum Geology*, **22**, 245–256, https://doi.org/10.1016/j.marpetgeo.2004.10.019

Laberg, J.S. and Camerlenghi, A. 2008. The significance of contourites for submarine slope stability. *Developments in Sedimentology*, **60**, 537–556, https://doi.org/10.1016/S0070-4571(08)10025-5

Laberg, J.S. and Vorren, T.O. 2000. The Trænadjupet Slide, offshore Norway – morphology, evacuation and triggering mechanisms. *Marine Geology*, **171**, 95–114, https://doi.org/10.1016/S0025-3227(00)00112-2

Laberg, J.S., Dahlgren, T., Vorren, T.O., Haflidason, H. and Bryn, P. 2001. Seismic analyses of Cenozoic contourite drift development in the Northern Norwegian Sea. *Marine Geophysical Researches*, **22**, 401–416, https://doi.org/10.1023/A:1016347632294

Laberg, J.S., Vorren, T.O. *et al*. 2002. Late Quaternary paleoenvironment and chronology in the Trænadjupet Slide area offshore Norway. *Marine Geology*, **188**, 35–60, https://doi.org/10.1016/S0025-3227(02)00274-8

Laberg, J.S., Vorren, T.O. and Mienert, J. 2003. Preconditions leading to the Holocene Trænadjupet Slide offshore Norway. *In*: Locat, J. and Mienert, J. (eds) *Submarine Mass Movements and Their Consequences*. Advances in Natural and Technological Hazards Research, **19**, Springer, Dordrecht, 247–254, https://doi.org/10.1007/978-94-010-0093-2_28

L'Heureux, J.-S., Longva, O. *et al*. 2012. Identification of weak layers and their role for the stability at Finneidfjord, Northern Norway. *In*: Yamada, Y., Kawamura, K. *et al*. (eds) *Submarine Mass Movements and Their Consequences*. Advances in Natural and Technological Hazard

Research, **31**, Springer, Dordrecht, 321–330, https://doi.org/10.1007/978-94-007-2162-3_29

Lindberg, B., Laberg, J.S. and Vorren, T.O. 2004. The Nyk Slide – morphology, progression, and age of a partly buried submarine slide offshore northern Norway. *Marine Geology*, **213**, 277–289, https://doi.org/10.1016/j.margeo.2004.10.010

Long, D., Bulat, J. and Stoker, M.S. 2004. Sea bed morphology of the Faroe-Shetland Channel derived from 3D seismic datasets. *Geological Society, London, Memoirs*, **29**, 53–61, https://doi.org/10.1144/GSL.MEM.2004.029.01.06

Lüdmann, T., Wiggershaus, S., Betzler, C. and Hübscher, C. 2012. Southwest Mallorca Island: a cool-water carbonate margin dominated by drift deposition associated with giant mass wasting. *Marine Geology*, **307-310**, 73–87, https://doi.org/10.1016/j.margeo.2011.09.008

Madhusudhan, B.N., Clare, M.A., Clayton, C.R.I. and Hunt, J.E. 2017. Geotechnical profiling of deep-ocean sediments at the AFEN submarine slide complex. *Quarterly Journal of Engineering Geology and Hydrology*, **50**, 148–157, https://doi.org/10.1144/qjegh2016-057

Maldonado, A., Barnolas, A. *et al*. 2005. Miocene to recent contourite drifts development in the northern Weddell Sea (Antarctica). *Global and Planetary Change*, **45**, 99–129, https://doi.org/10.1016/j.gloplacha.2004.09.013

Marion, D., Nur, A., Yin, H. and Han, D. 1992. Compressional velocity and porosity in sand-clay mixtures. *Geophysics*, **57**, 554–563, https://doi.org/10.1190/1.1443269

Maslin, M., Owen, M., Day, S. and Long, D. 2004. Linking continental-slope failures and climate change: testing the clathrate gun hypothesis. *Geology*, **32**, 53–56, https://doi.org/10.1130/G20114.1

Masson, D.G. 2001. Sedimentary processes shaping the eastern slope of the Faeroe-Shetland Channel. *Continental Shelf Research*, **21**, 825–857, https://doi.org/10.1016/S0278-4343(00)00115-1

Masson, D.G. Wynn, R.B. and Bett, B.J. 2004. Sedimentary environment of the Faroe-Shetland and Faroe Bank Channels, north-east Atlantic, and the use of bedforms as indicators of bottom current velocity in the deep ocean. *Sedimentology*, **51**, 1207–1241, https://doi.org/10.1111/j.1365-3091.2004.00668.x

Masson, D.G., Harbitz, C.B., Wynn, R.B., Pedersen, G. and Løvholt, F. 2006. Submarine landslides: processes, triggers and hazard prediction. *Philosophical Transactions: Mathematical, Physical and Engineering Sciences*, **354**, 2009–2039, https://doi.org/10.1098/rsta.2006.1810

Mattingsdal, R., Knies, J., Andreassen, K., Fabian, K., Husum, K., Grøsfjeld, K. and De Schepper, S. 2014. A new 6 Myr stratigraphic framework for the Atlantic-Arctic Gateway. *Quaternary Science Reviews*, **92**, 170–178, https://doi.org/10.1016/j.quascirev.2013.08.022

McCave, I.N. and Tucholke, B.E. 1986. Deep current controlled sedimentation in the western North Atlantic. *In*: Vogt, P.R. and Tucholke, B.E. (eds) *The Western North Atlantic Region*. Geology of North America, Volume **M**, 451–468.

Micallef, A., Berndt, C., Masson, D.G. and Stow, D.A. 2008. Scale invariant characteristics of the Storegga

Slide and implications for large-scale submarine mass movements. *Marine Geology*, **247**, 46–60, https://doi.org/10.1016/j.margeo.2007.08.003

Minisini, D., Trincardi, F., Asioli, A., Canu, M. and Foglini, F. 2007. Morphologic variability of exposed mass-transport deposits on the eastern slope of Gela Basin (Sicily channel). *Basin Research*, **19**, 217–240, https://doi.org/10.1111/j.1365-2117.2007.00324.x

Miramontes, E., Cattaneo, A. *et al*. 2016. The Pianosa Contourite Depositional System (Northern Tyrrhenian Sea): drift morphology and Plio-Quaternary stratigraphic evolution. *Marine Geology*, **378**, 20–42, https://doi.org/10.1016/j.margeo.2015.11.004

Miramontes, E., Garziglia, S., Sultan, N., Jouet, G. and Cattaneo, A. 2018. Morphological control of slope instability in contourites: a geotechnical approach. *Landslides*, **15**, 1085–1095, https://doi.org/10.1007/s10346-018-0956-6

Mulder, T., Ducassou, E. *et al*. 2012. New insights into the morphology and sedimentary processes along the western slope of Great Bahama Bank. *Geology*, **40**, 603–606, https://doi.org/10.1130/G32972.1

Nielsen, T., Rasmussen, T.L., Ceramicola, S. and Kuijpers, A. 2007. Quaternary sedimentation, margin architecture and ocean circulation variability around the Faroe Islands, North Atlantic. *Quaternary Science Reviews*, **26**, 1016–1036, https://doi.org/10.1016/j.quascirev.2006.12.005

Normandeau, A., Campbell, D.C., Piper, D.J. and Jenner, K.A. 2019. Are submarine landslides an underestimated hazard on the western North Atlantic passive margin? *Geology*, **47**, 848–852, https://doi.org/10.1130/G46201.1

Perez, L., Garcá-Rodríguez, F. and Hanebuth, T.J.J. 2016. Variability in terrigenous sediment supply offshore of the Río de la Plata (Uruguay) recording the continental climatic history over the past 1200 years. *Climate of the Past*, **12**, 623–634, https://doi.org/10.5194/cp-12-623-2016

Piper, D.J.W. 2005. Late Cenozoic evolution of the continental margin of eastern Canada. *Norwegian Journal of Geology*, **85**, 305–318.

Pope, E.L., Talling, P.J., Urlaub, M., Hunt, J.E., Clare, M.A. and Challenor, P. 2015. Are large submarine landslides temporally random or do uncertainties in available age constraints make it impossible to tell? *Marine Geology*, **369**, 19–33, https://doi.org/10.1016/j.margeo.2015.07.002

Powrie, W. 2013. *Soil Mechanics: Concepts and Applications*. 3rd edn. CRC Press, Taylor & Francis.

Preu, B., Hernández-Molina, F.J. *et al*. 2013. Morphosedimentary and hydrographic features of the northern Argentine margin: the interplay between erosive, depositional and gravitational processes and its conceptual implications. *Deep-Sea Research I*, **75**, 157–174, https://doi.org/10.1016/j.dsr.2012.12.013

Prieto, M.I., Moscardelli, L. and Wood, L.J. 2016. Exploring the influence of deepwater currents as potential triggers for slope instability. *In*: Lamarche, G., Mountjoy, J. *et al*. (eds) *Submarine Mass Movements and their Consequences*. Advances in Natural and Technological Hazards Research, **41**, Springer, Cham, 331–338, https://doi.org/10.1007/978-3-319-20979-1_33

Principaud, M., Mulder, T., Gillet, H. and Borgomano, J. 2015. Large-scale carbonate submarine mass-wasting along the northwestern slope of the Great Bank (Bahamas): morphology, architecture, and mechanisms. *Sedimentary Geology*, **317**, 27–42, https://doi.org/10.1016/j.sedgeo.2014.10.008

Rahmstorf, S. 2002. Ocean circulation and climate during the last 120,000 years. *Nature*, **419**, 207–214, https://doi.org/10.1038/nature01090

Rashid, H., MacKillop, K., Sherwin, J., Piper, D.J.W., Marche, B. and Vermooten, M. 2017. Slope instability on a shallow contourite-dominated continental margin, southeastern Grand Banks, eastern Canada. *Marine Geology*, **393**, 203–215, https://doi.org/10.1016/j.margeo.2017.01.001

Rasmussen, T.L., Thomsen, E., van Weering, T.C.E. and Labeyrie, L. 1996. Rapid changes in surface and deep water conditions at the Faeroe Margin during the last 58,000 years. *Paleoceanography*, **11**, 757–771, https://doi.org/10.1029/96PA02618

Rasmussen, T.L., Thomsen, E. and van Weering, T.C.E. 1998. Cyclic sedimentation of the Faeroe Drift 53-10 ka BP related to climatic variations. *Geological Society, London, Special Publications*, **129**, 255–267, https://doi.org/10.1144/GSL.SP.1998.129.01.16

Rasmussen, T.L., Bäckström, D. *et al*. 2002. The Faroe-Shetland Gateway: late Quaternary water mass exchange between the Nordic seas and the northeastern Atlantic. *Marine Geology*, **188**, 165–192, https://doi.org/10.1016/S0025-3227(02)00280-3

Rebesco, M. and Stow, D. 2001. Seismic expression of contourites and related deposits: a preface. *Marine Geophysical Researches*, **22**, 303–308, https://doi.org/10.1023/A:1016316913639

Rebesco, M., Hernández-Molina, F.J., Van Rooij, D. and Wåhlin, A. 2014. Contourites and associated sediments controlled by deep-water circulation processes: state-of-the-art and future considerations. *Marine Geology*, **352**, 111–154, https://doi.org/10.1016/j.margeo.2014.03.011

Ren, X.W. and Santamarina, J.C. 2018. The hydraulic conductivity of sediments: a pore size perspective. *Engineering Geology*, **233**, 48–54, https://doi.org/10.1016/j.enggeo.2017.11.022

Revil, A. and Cathles, III, L.M. 1999. Permeability of shaly sands. *Water Resource Research*, **35**, 651–662, https://doi.org/10.1029/98WR02700

Ritchie, J.D., Johnson, H. and Kimbell, G.S. 2003. The nature and age of Cenozoic contractional deformation within the NE Faroe-Shetland Basin. *Marine and Petroleum Geology*, **20**, 399–409, https://doi.org/10.1016/S0264-8172(03)00075-8

Ritchie, J.D., Johnson, H., Quinn, M.F. and Gatliff, R.W. 2008. The effects of Cenozoic compression within the Faroe-Shetland Basin and adjacent areas. *Geological Society, London, Special Publications*, **306**, 121–136, https://doi.org/10.1144/SP306.5

Roberts, D.G., Thompson, M., Mitchener, B., Hossack, J., Carmichael, S. and Bjørnseth, H.-M. 1999. Palaeozoic to Tertiary rift and basin dynamics: mid-Norway to the Bay of Biscay – a new context for hydrocarbon prospectivity in the deep water frontier. *Geological Society, London, Petroleum Geology Conference Series*, **5**, 7–40, https://doi.org/10.1144/0050007

Röhl, U. and Abrams, L.J. 2000. High-resolution, down-hole and non-destructive core measurements from Sites 999 and 1001 in the Caribbean Sea: application to the Late Paleocene Thermal Maximum. *In*: Leckie, R.M., Sigurdsson, H., Acton, G.D. and Draper, G. (eds) *Proceedings of the ODP, Scientific Results*, **165**. Ocean Drilling Program, College Station, TX, 191–203.

Rothwell, R.G. and Rack, F.R. 2006. New techniques in sediment core analysis: an introduction. *Geological Society, London, Special Publications*, **267**, 1–29, https://doi.org/10.1144/GSL.SP.2006.267.01.01

Rumph, B., Reaves, C.M., Orange, V.G. and Robinson, D.L. 1993. Structuring and transfer zones in the Faeroe Basin in a regional tectonic context. *Geological Society, London, Petroleum Geology Conference Series*, **4**, 999–1009, https://doi.org/10.1144/0040999

Saunders, P.M. 1990. Cold outflow from the Faroe Bank Channel. *Journal of Physical Oceanography*, **20**, 29–43, https://doi.org/10.1175/1520-0485(1990)020<0029:COFTFB>2.0.CO;2

Sheskin, D.J. 2011. *Handbook of Parametric and Non-parametric Statistical Procedures*. 5th edn. CRC Press, Taylor & Francis.

Shipp, R.C., Weimer, P. and Posamentier, H.W. (eds) 2011. *Mass-Transport Deposits in Deepwater Settings*. SEPM Special Publications, **96**. SEPM Society for Sedimentary Geology, https://doi.org/10.2110/sepmsp.096

Smallwood, J.R. and Gill, C.E., 2002. The rise and fall of the Faroe-Shetland Basin: evidence from seismic mapping of the Balder Formation. *Journal of the Geological Society, London*, **159**, 627–630, https://doi.org/10.1144/0016-764902-064

Smith, S.V., Buddemeier, R.W., Redalje, R.C. and Houck, J.E., 1979. Strontium-calcium thermometry in coral skeletons. *Science*, **207**, 404–407, https://doi.org/10.1126/science.204.4391.404

Solheim, A., Berg, K., Forsberg, C.F. and Bryn, P. 2005. The Storegga Slide complex: repetitive large scale sliding with similar cause and development. *Marine and Petroleum Geology*, **22**, 97–107, https://doi.org/10.1016/j.marpetgeo.2004.10.013

Stoker, M.S., Akhurst, M.C., Howe, J.A. and Stow, D.A.V. 1998. Sediment drifts and contourites on the continental margin off northwest Britain. *Sedimentary Geology*, **15**, 33–51, https://doi.org/10.1016/S0037-0738(97)00086-9

Stoker, M.S., Nielsen, T., van Weering, T.C.E. and Kuijpers, A. 2002. Towards an understanding of the Neogene tectonostratigraphic framework of the NE Atlantic margin between Ireland and the Faroe Islands. *Marine Geology*, **188**, 233–248, https://doi.org/10.1016/S0025-3227(02)00282-7

Stoker, M.S., Hoult, R.J. *et al.* 2005. Sedimentary and oceanographic responses to early Neogene compression on the NW European margin. *Marine and Petroleum Geology*, **22**, 1031–1044, https://doi.org/10.1016/j.marpetgeo.2005.01.009

Stow, D.A.V. and Holbrook, J.A. 1984. Hatton Drift contourites, northeast Atlantic, Deep Sea Drilling Project Leg 81. *Initial Reports of the Deep Sea Drilling Project*, **81**. US Government Printing Office, Washington, DC, 695–699, https://doi.org/10.2973/dsdp.proc.81.125.1984

Stow, D.A.V., Faugères, J.C., Howe, J.A., Pudsey, C.J. and Viana, A.R. 2002. Bottom currents, contourites and deep-sea sediment drifts: current state-of-the-art. *Geological Society, London, Memoirs*, **22**, 7–20, https://doi.org/10.1144/GSL.MEM.2002.022.01.02

Talling, P.J., Clare, M.L., Urlaub, M., Pope, E., Hunt, J.E. and Watt, S.F. 2014. Large submarine landslides on continental slopes: geohazards, methane release, and climate change. *Oceanography*, **27**, 32–45, https://doi.org/10.5670/oceanog.2014.38

Terzaghi, K. 1925. *Erdbaumechanik auf Bodenphysikalischer Grundlage*. F. Deuticke, Leipzig.

Thomson, J., Crudeli, D., De Lange, G., Slomp, C.P., Erba, E., Corselli, C. and Calvert, S.E. 2004. *Florisphaera profunda* and the origin and diagenesis of carbonate phases in eastern Mediterranean sapropel units. *Paleoceanography*, **19**, PA3003, https://doi.org/10.1029/2003PA000976

Tournadour, E., Mulder, T., Borgomano, J., Hanquiez, V., Ducassou, E. and Gillet, H. 2015. Origin and architecture of a Mass Transport Complex on the northwest slope of Little Bahama Bank (Bahamas): relations between off-bank transport, bottom current sedimentation and submarine landslides. *Sedimentary Geology*, **317**, 9–26, https://doi.org/10.1016/j.sedgeo.2014.10.003

Turner, J.D. and Scrutton, R.A. 1993. Subsidence patterns in western margin basins: evidence from the Faeroe-Shetland Basin. *Geological Society, London, Petroleum Geology Conference Series*, **4**, 975–983, https://doi.org/10.1144/0040975

Turrell, W.R., Slesser, G., Adams, R.D., Payne, R. and Gillibrand, P.A. 1999. Decadal variability in the composition of Faroe Shetland Channel bottom water. *Deep-Sea Research I*, **46**, 1–25, https://doi.org/10.1016/S0967-0637(98)00067-3

Urgeles, R. and Camerlenghi, A. 2013. Submarine landslides of the Mediterranean Sea: trigger mechanisms, dynamics, and frequency-magnitude distribution. *Journal of Geophysical Research: Earth Surface*, **118**, 2600–2618, https://doi.org/10.1002/2013JF002720

Urlaub, M., Talling, P.J. and Masson, D.G. 2013. Timing and frequency of large submarine landslides: implications for understanding triggers and future geohazard. *Quaternary Science Reviews*, **72**, 63–82, https://doi.org/10.1016/j.quascirev.2013.04.020

Urlaub, M., Talling, P. and Clare, M. 2014. Sea-level-induced seismicity and submarine landslide occurrence: comment. *Geology*, **42**, 337, https://doi.org/10.1130/G35254C.1

Van Raaphorst, W., Malschaert, H., van Haren, H., Boer, W. and Brummer, G.-J. 2001. Cross-slope zonation of erosion and deposition in the Faeroe-Shetland Channel. *North Atlantic Ocean. Deep-Sea Research I*, **48**, 567–591, https://doi.org/10.1016/S0967-0637(00)00052-2

Van Weering, Tj.C.E. and de Rijk, S. 1991. Sedimentation and climate-induced sediments on Feni Ridge, Northeast Atlantic Ocean. *Marine Geology*, **101**, 49–69, https://doi.org/10.1016/0025-3227(91)90062-9

Van Weering, T.C.E., Nielsen, T., Kenyon, N.H., Akentieva, K. and Kuijpers, A.H. 1998. Sediments and sedimentation at the NE Faeroe continental

margin; contourites and large-scale sliding. *Marine Geology*, **152**, 159–176, https://doi.org/10.1016/S0025-3227(98)00069-3

Vanneste, M., Mienert, J. and Bünz, S. 2006. The Hinlopen Slide: a giant, submarine slope failure on the northern Svalbard margin, Arctic Ocean. *Earth and Planetary Science Letters*, **245**, 373–388, https://doi.org/10.1016/j.epsl.2006.02.045

Vardy, M.E., L'Heureux, J.-S. *et al.* 2012. Multidisciplinary investigation of a shallow near-shore landslides, Finneidfjord, Norway. *Near Surface Geophysics*, **10**, 267–277, https://doi.org/10.3997/1873-2012022

Verdicchio, G. and Trincardi, F. 2008. Mediterranean shelf-edge muddy contourites: examples from the Gela and South Adriatic basins. *Geo-Marine Letters*, **28**, 137–151, https://doi.org/10.1007/s00367-007-0096-9

Volpi, V., Camerlenghi, A., Hillenbrand, C.D., Rebesco, M. and Ivaldi, R. 2003. Effects of biogenic silica on sediment compaction and slope stability on the Pacific margin of the Antarctic Peninsula. *Basin Research*, **15**, 339–363, https://doi.org/10.1046/j.1365-2117.2003.00210.x

Volpi, V., Amblas, D., Camerlenghi, A., Canals, M., Rebesco, M. and Urgeles, R. 2011. Late Neogene to recent seafloor instability on the deep pacific margin of the Antarctic Peninsula. *SEPM Special Publications*, **96**, 161–177, https://doi.org/10.2110/sepmsp.096.161

Weltje, G.J. and Tjallingii, R. 2008. Calibration of XRF core scanners for quantitative geochemical logging of sediment cores: theory and application. *Earth and Planetary Science Letters*, **274**, 423–438, https://doi.org/10.1016/j.epsl.2008.07.054

Wilson, C.K., Long, D. and Bulat, J. 2003. The Afen Slide – A multistage slope failure in the Faroe-Shetland Channel. *In*: Locat, J. and Mienert, J. (eds) *Submarine Mass Movements and Their Consequences*. Advances in Natural and Technological Hazards Research, **19**, Springer, Dordrecht, 317–324, https://doi.org/10.1007/978-94-010-0093-2_35

Wilson, C.K., Long, D. and Bulat, J. 2004. The morphology, setting and processes of the Afen Slide. *Marine Geology*, **213**, 149–167, https://doi.org/10.1016/j.margeo.2004.10.005

Wilson, C.K., Bulat, J. and Long, D. 2005. The Afen Slide. British Geological Survey Commissioned Report **CR/05/003**.

Winkelmann, D., Geissler, W., Schneider, J. and Stein, R. 2008. Dynamics and timing of the Hinlopen/Yermak Megaslide north of Spitsbergen, Arctic Ocean. *Marine Geology*, **250**, 34–50, https://doi.org/10.1016/j.margeo.2007.11.013